Full-Wave Analysis of Coupling Between Combline Resonators and Its Application to Combline Filters With Canonical Configurations

Mahmoud El Sabbagh, *Student Member, IEEE*, Kawthar A. Zaki, *Fellow, IEEE*, Hui-Wen Yao, *Senior Member, IEEE*, and Ming Yu, *Senior Member, IEEE*

***Abstract*—Resonant frequencies and coupling coefficient between two combline cavities, in the presence of other cavities, are obtained accurately using the mode-matching technique. The effect of iris dimensions and position on the electric and magnetic coupling is rigorously investigated. The corresponding data for two isolated cavities are included for comparison. The adjacent and nonadjacent couplings are rigorously investigated for different configurations of three coupled cavities. A four-pole slot-coupled elliptic combline filter is designed.**

***Index Terms*—Combline filters, electromagnetic coupling.**

I. Introduction

THE conventional combline filter consists of a set of metal bars, spaced, grounded at one end, and loaded by lumped capacitors or open circuited at the other side. The comblines are viewed as coupled TEM-mode transmission lines [1]. By increasing the electrical length of the resonators, selectivity on the high side of the passband increases, but decreases on the low side. To design combline filters with narrow bandwidth, with transmission zeros to improve the selectivity or with small spacing between resonators to miniaturize the dimensions, irises between resonators are then needed. The irises control the couplings, which could be either magnetic or electric. Accurate determination of coupling between two isolated combline cavities has been reported [2]–[4]. However, there is no accurate modeling of the coupling between two cavities in the presence of other couplings, particularly in a canonical configuration. In this paper, a rigorous method using the mode-matching technique is applied to calculate the resonant frequencies and the slot coupling coefficients of combline cavities in the presence of adjacent cavities including the configurations usually seen in canonical filters. The results obtained are used to design a four-pole elliptic function filter. The effect of nonadjacent coupling between combline cavities is also rigorously investigated.

Manuscript received March 30, 2001; revised July 13, 2001.

M. El Sabbagh and K. A. Zaki are with the Department of Electrical and Computer Engineering, University of Maryland at College Park, College Park, MD 20742 USA.

H.-W. Yao is with the Orbital Sciences Corporation, Germantown, MD 20301 USA.

M. Yu is with ComDev Inc., Cambridge, ON Canada N1R 7H6.

Publisher Item Identifier S 0018-9480(01)10453-9.

II. Modeling

A. Building Blocks Modeling

The structure of iris coupled combline cavities under consideration is shown in Fig. 1. The structure that is usually seen in canonical filters can be modeled by cascading the building blocks shown in Fig. 2. From these blocks, the slot discontinuity is easily modeled using the full-wave mode-matching technique. Therefore, the key problem of modeling slot coupled combline cavities, in the presence of other couplings in the canonical configuration, is to compute the scattering matrices of a cylindrical metal post in a right bend and a T-junction. To do this, the symmetrical (all ports are assumed to have the same cross-sectional dimensions) cross waveguide junction, shown in Fig. 2(a), is analyzed first [11]. By considering its symmetrical properties, the generalized scattering matrix of the cross waveguide junction can be derived from four sets of two ports generalized scattering matrices obtained by bisecting the junction at the symmetry planes using combination of perfect electric wall (PEW) and perfect magnetic wall (PMW). The following four cases are analyzed: PEW–PEW, PEW–PMW, PMW–PEW, and PMW–PMW, where the first wall is placed at the vertical plane of symmetry and the second wall is placed at the horizontal plane of symmetry, as shown in Fig. 3. Since the cases of PMW–PEW or PEW–PMW are the same, it is sufficient to analyze three different cases of two-port structures [11] from which the generalized scattering matrix of the cross junction $[S_4^G]$ is obtained using (1), shown at the bottom of the following page.

Each element of the matrix is a generalized matrix, e.g., S_{ij}^{me} represents the generalized scattering matrix of the right-angle bend (quarter of the structure) in case of a vertical PMW (represented by superscript m), horizontal PEW (represented by superscript e), and so on for other elements.

The generalized scattering matrices of the T-junction $[S^T]$ and the right-angle bend $[S^B]$ are obtained by placing short circuits at one or two adjacent ports, respectively. Similarly, by placing short circuits at two opposite ports, the generalized scattering matrix $[S^R]$ of a post inside a rectangular waveguide is obtained. A cascading procedure using generalized scattering matrices [6], [13] is employed with proper terminating conditions to calculate the resonant frequency and the coupling coefficient between two combline cavities in the presence of other couplings.

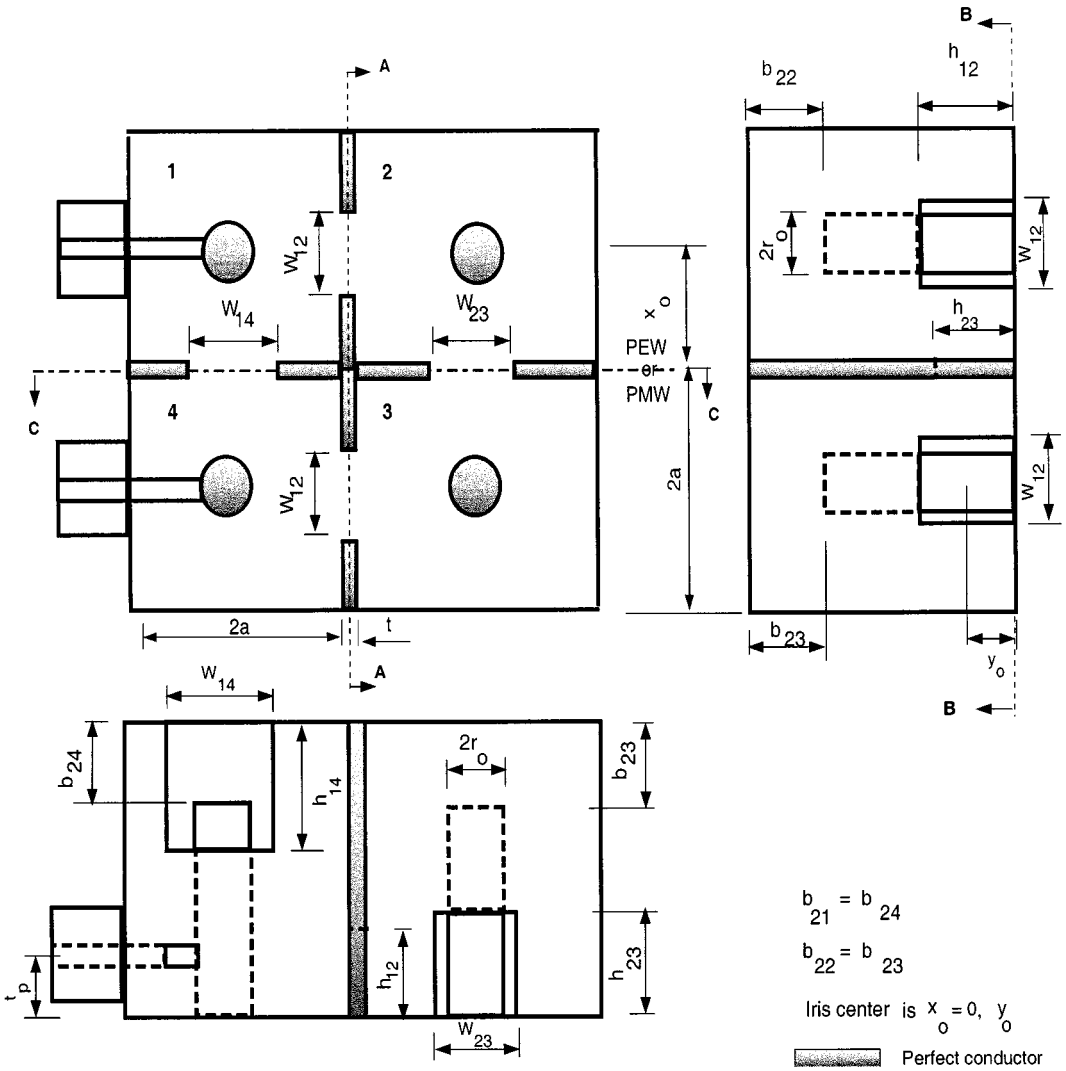

Fig. 1. Top and side views of four-pole elliptic-function combline filter. Dimensions in this figure: $2a = 0.75$ in, $b = 1.315$ in, $r_o = 0.115$ in, $t = 0.1$ in.

B. Iris Coupled Combline Cavities in the Presence of Other Couplings in Canonical Configurations

Fig. 4 shows the model of the structure of Fig. 1 using the building blocks of Fig. 2. In this model, the input/output couplings are neglected and the input/output ports are short circuited. In the model, a PEW or a PMW is placed only between the two combline cavities required to compute their coupling. The other two cavities are detuned off resonance. The two resonant frequencies f_e and f_m (corresponding to PEW and PMW, respectively) are computed. The coupling is obtained in terms of f_e and f_m by using (2) [4] as follows:

$$k = \frac{f_e^2 - f_m^2}{f_e^2 + f_m^2} \tag{2}$$

$$\frac{1}{2}\left(\begin{array}{cc|cc|cc|cc}
S_{11}^{mm}+S_{11}^{em} & 0 & S_{11}^{mm}-S_{11}^{em} & 0 & S_{12}^{mm} & S_{12}^{em} & S_{12}^{mm} & S_{12}^{em} \\
0 & S_{11}^{me}+S_{11}^{ee} & 0 & S_{11}^{me}-S_{11}^{ee} & S_{12}^{me} & S_{12}^{ee} & -S_{12}^{me} & -S_{12}^{ee} \\
\hline
S_{11}^{mm}-S_{11}^{em} & 0 & S_{11}^{mm}+S_{11}^{em} & 0 & S_{12}^{mm} & -S_{12}^{em} & S_{12}^{mm} & -S_{12}^{em} \\
0 & S_{11}^{me}-S_{11}^{ee} & 0 & S_{11}^{me}+S_{11}^{ee} & S_{12}^{me} & -S_{12}^{ee} & -S_{12}^{me} & S_{12}^{ee} \\
\hline
S_{21}^{mm} & S_{21}^{me} & S_{21}^{mm} & S_{21}^{me} & S_{22}^{mm}+S_{22}^{me} & 0 & S_{22}^{mm}-S_{22}^{me} & 0 \\
S_{21}^{em} & S_{21}^{ee} & -S_{21}^{em} & -S_{21}^{ee} & 0 & S_{22}^{em}+S_{22}^{ee} & 0 & S_{22}^{em}-S_{22}^{ee} \\
\hline
S_{21}^{mm} & S_{21}^{me} & S_{21}^{mm} & S_{21}^{me} & S_{22}^{mm}-S_{22}^{me} & 0 & S_{22}^{me}+S_{22}^{mm} & 0 \\
S_{21}^{em} & -S_{21}^{ee} & -S_{21}^{em} & S_{21}^{ee} & 0 & S_{22}^{em}+S_{22}^{ee} & 0 & S_{22}^{em}+S_{22}^{ee}
\end{array}\right) \tag{1}$$

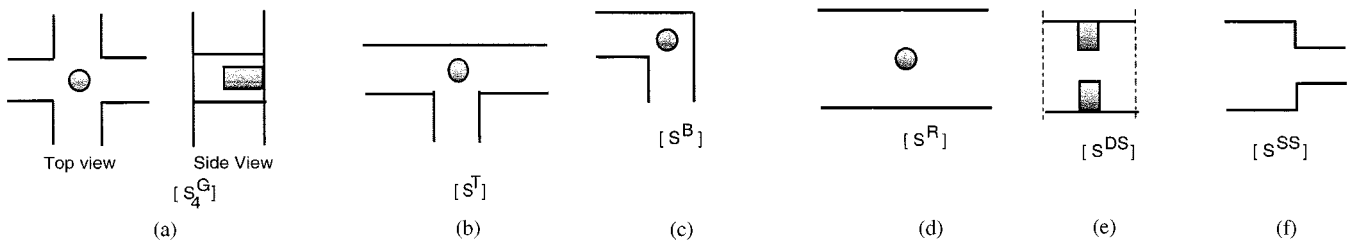

Fig. 2. Building blocks. (a) Four-port junction $[S_4^G]$. (b) T-junction $[S^T]$. (c) Right-angle bend $[S^B]$. (d) Double step in rectangular waveguide $[S^{DS}]$. (e) Single step in rectangular waveguide $[S^{SS}]$.

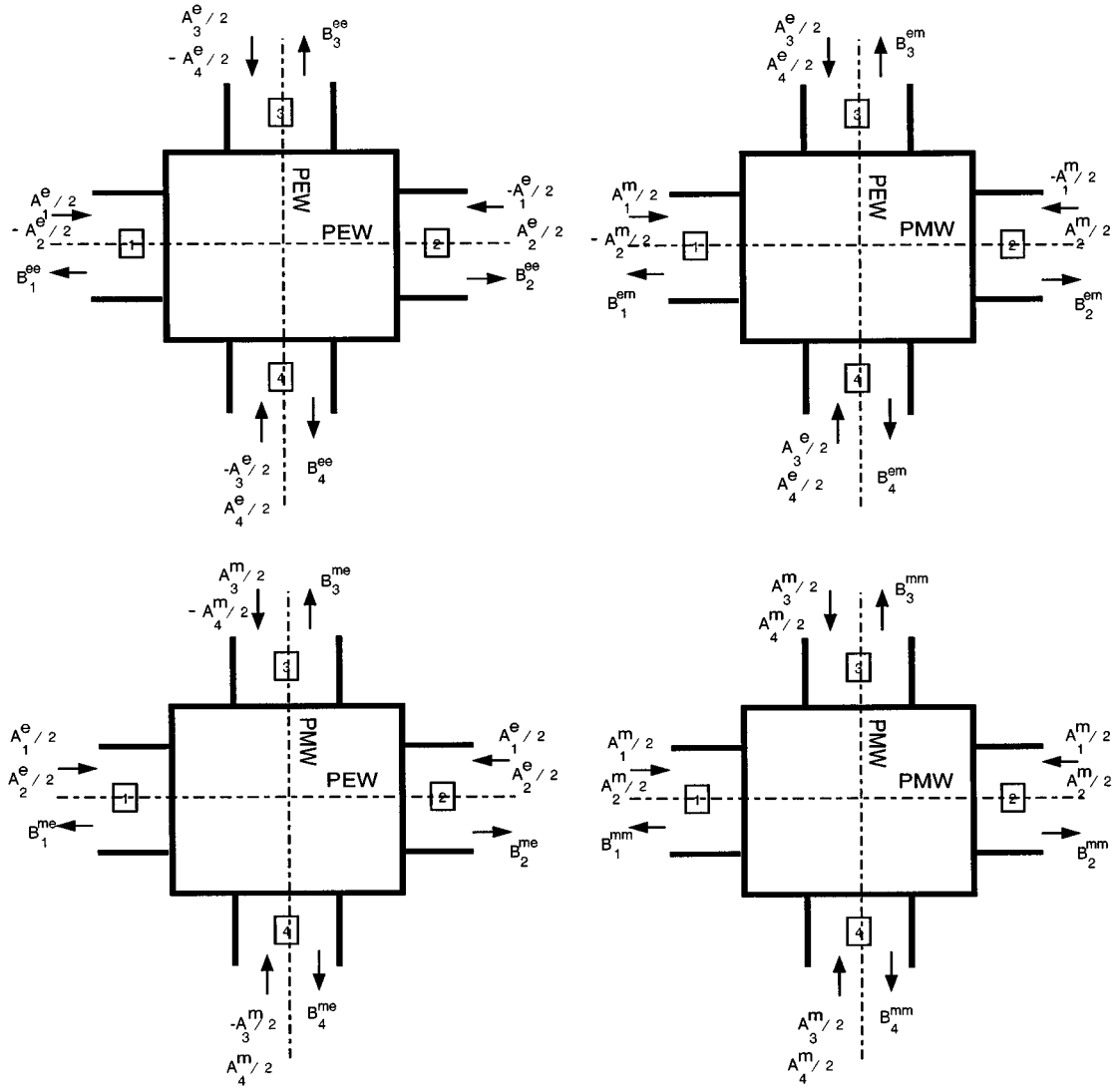

Fig. 3. Crossed waveguide junction (the different cases of quarter structures with corresponding inputs and outputs are shown).

and the resonant frequency f_o of each cavity is given by

$$f_o = \sqrt{f_e f_m}. \tag{3}$$

Equations (2) and (3) are based on the assumption that the two coupled cavities are identical. If this is not the case, short- and open-circuit conditions have to be realized at one end of the network successively to obtain two zeros (f_{z1} and f_{z2}) and one pole (f_p), respectively, from which the coupling coefficient can be computed as [2]

$$k_{12}^2 = 1 - \frac{f_1^2 + f_p^2}{f_{z1}^2 + f_{z2}^2} \tag{4}$$

$$f_1^2 = \frac{(f_p f_{z1} f_{z2})^2}{f_p^2\left(f_{z1}^2 + f_{z2}^2\right) - f_{z1}^2 f_{z2}^2}. \tag{5}$$

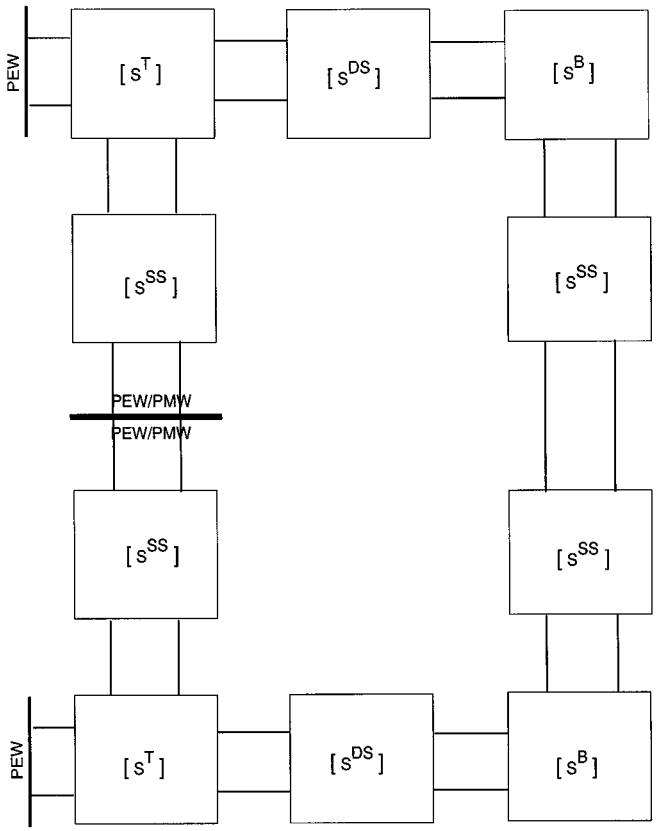

Fig. 4. S-matrix representation of the structure of Fig. 1.

C. Nonadjacent Coupling Between Combline Cavities

During the tuning process of combline filters, it is found that there is an undesired coupling between nonadjacent cavities. This kind of coupling is responsible of the deviation of the filter response from the one obtained from the synthesis procedure. Different configurations of three coupled cavities are shown in Fig. 5, where the coupling structures 1 and 2 could be any waveguide discontinuities or their combinations. For these configurations, there exist the adjacent couplings between cavities 1 and 2 (k_{12}) and between cavities 2 and 3 (k_{23}) in addition to the nonadjacent coupling (k_{13}) between cavities 1 and 3. Fig. 5(e) shows the equivalent circuit of three nonadjacent coupled cavities near a resonant frequency [4]. The coupling k_{12} and cavities 1 and 2 resonant frequencies are given by [4]

$$k_{12}^2 = 1 - \frac{f_1^2 + f_p^2}{f'^2_{z1} + f'^2_{z2}} \tag{6}$$

$$f_1^2 = \frac{\left(f_p f'_{z1} f'_{z2}\right)^2}{f_p^2\left(f'^2_{z1} + f'^2_{z2}\right) - f'^2_{z1} f'^2_{z2}} \tag{7}$$

$$f_2 = f_p \tag{8}$$

where f'_{z1} and f'_{z2} are the two natural frequencies when the short circuit is placed at the A–A-plane and the open-circuit condition is placed at the B–B-plane; f_p is the resonant frequency when the open circuit conditions are applied at both the A–A- and B–B-planes. Switching the input port at plane B–B and repeating the above procedure, the coupling k_{23} and cavity 3 resonant frequency are then given by

$$k_{23}^2 = 1 - \frac{f_3^2 + f_p^2}{f''^2_{z1} + f''^2_{z2}} \tag{9}$$

$$f_3^2 = \frac{\left(f_p f''_{z1} f''_{z2}\right)^2}{f_p^2\left(f''^2_{z1} + f''^2_{z2}\right) - f''^2_{z1} f''^2_{z2}} \tag{10}$$

where f''_{z1} and f''_{z2} are the natural frequencies when the open circuit is placed at the A–A-plane and the short-circuit condition is placed at the B–B-plane. From the knowledge of the resonant frequency of each cavity, as well as the adjacent couplings, the nonadjacent coupling is obtained by placing a short-circuit condition at both the A–A- and B–B-planes. Three natural frequencies, i.e., f_{z1}, f_{z2} and f_{z3}, will exist and satisfy (11) from which the nonadjacent coupling is obtained as follows:

$$\begin{aligned} &f_2 f_{zi}^2 \lambda_2(f_{zi}) k_{13}^2 - 2 f_{zi}^3 k_{12} k_{23} k_{13} + f_1 f_{zi}^2 \lambda_1(f_{zi}) k_{23}^2 \\ &\quad + f_3 f_{zi}^2 \lambda_3 t(f_{zi}) k_{12}^2 f_1 f_2 f_3 \lambda_1(f_{zi}) \lambda_2(f_{zi}) \lambda_3(f_{zi}) \\ &\quad = 0, \qquad i = 1, 2, 3 \end{aligned} \tag{11}$$

where $\lambda_i(f)$ are defined as

$$\lambda_i(f) = \frac{f}{f_i} - \frac{f_i}{f}. \tag{12}$$

III. Numerical Results

A. Effect of Iris Height on Coupling

The effect of iris height (h) on the coupling and resonant frequency is investigated. The iris is either placed at the short-circuit end giving the positive coupling (magnetic coupling) or placed at the open end giving the negative coupling (electric coupling). The results obtained from the model proposed in Fig. 4, taking into account the adjacent irises effect, are compared to those obtained for two isolated cavities. Fig. 6(a) shows the effect of iris height on the positive coupling. The curve shows an increase of the coupling up to a maximum value at $h_{12}/b = 0.395$ then decreases with further increase of height. The figure also shows that the coupling obtained when taking the adjacent irises' effect is larger in value than the one obtained between two isolated cavities. Fig. 6(b) gives the variation of resonant frequency with iris height. The resonant frequency is decreasing up to a minimum resonant frequency at $h_{12}/b = 0.395$ and then starts to increase again with further increase of iris height. The figure shows that the loading effect of adjacent irises decreases the resonant frequency by 38.6 MHz from that of two isolated cavities. In the design of narrow-band filters, this shift of resonant frequency must be taken into account. The effect of iris height on the negative coupling is shown in Fig. 7(a) where the negative coupling increases as the iris height increases. The coupling has its maximum value at $h_{14}/b = 0.513$ and then decreases until it becomes positive coupling at $h_{14}/b = 0.67$. The coupling for two isolated cavities is close to the one obtained when taking the adjacent irises' effect into account. The corresponding resonant frequency curve is shown in Fig. 7(b), where the resonant frequency is increasing with the increase of the iris height up to a maximum value at

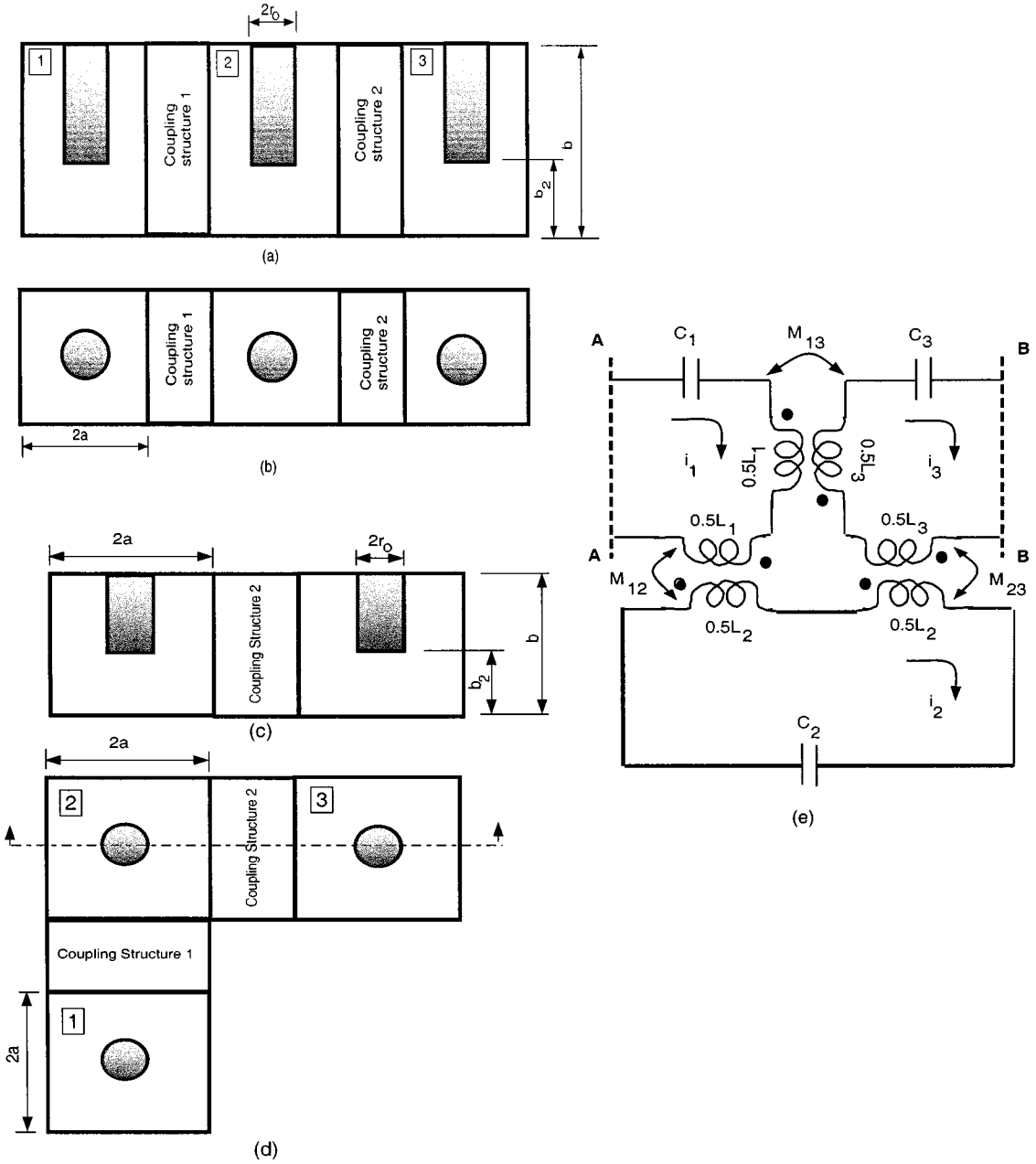

Fig. 5. Three combline cavities coupled through coupling irises including coupling rods. (a), (b) Side and top view, respectively, of three cavities lined up. (c), (d) Side and top view, respectively, of three cavities forming a corner. (e) Equivalent circuit model of three nonadjacent cavities.

$h_{14}/b = 0.557$, and then it starts to decrease again. The resonant frequency when taking the adjacent couplings' effect is reduced by 42.3 MHz from that between two isolated cavities.

B. Effect of Iris Width on Coupling

The results obtained from the accurate model in Fig. 4, taking into account the adjacent irises' effects, are compared to those obtained for two isolated cavities. Fig. 8(a) shows the variation of the magnetic coupling (positive coupling) with the iris width. Fig. 8(b) shows the variation of the resonant frequency versus the iris width. The loading effect when taken into account shows a difference of 40 MHz from that of two isolated cavities. Fig. 9(a) shows the effect of the iris width on the electric coupling (negative coupling). For very small width, the coupling is almost zero. As the width increases, the coupling increases up to a maximum value at $W/2a = 0.6$, after which the coupling decreases with further increase of the iris width. Fig. 9(b) shows the variation of the resonant frequency, for the case of negative coupling, versus the iris width. The resonant frequency increases with the increase of width up to a maximum value at $W/2a = 0.6$ after which the resonant frequency decreases with a further increase of the iris width. The curves also show that the loading effect due to the adjacent irises' effect is about a 41 MHz difference from the case of the two isolated cavities.

C. Effect of Post Gap on Negative Coupling

The effect of post gap variation on electric coupling is now investigated. The variation of the post gap is inversely related

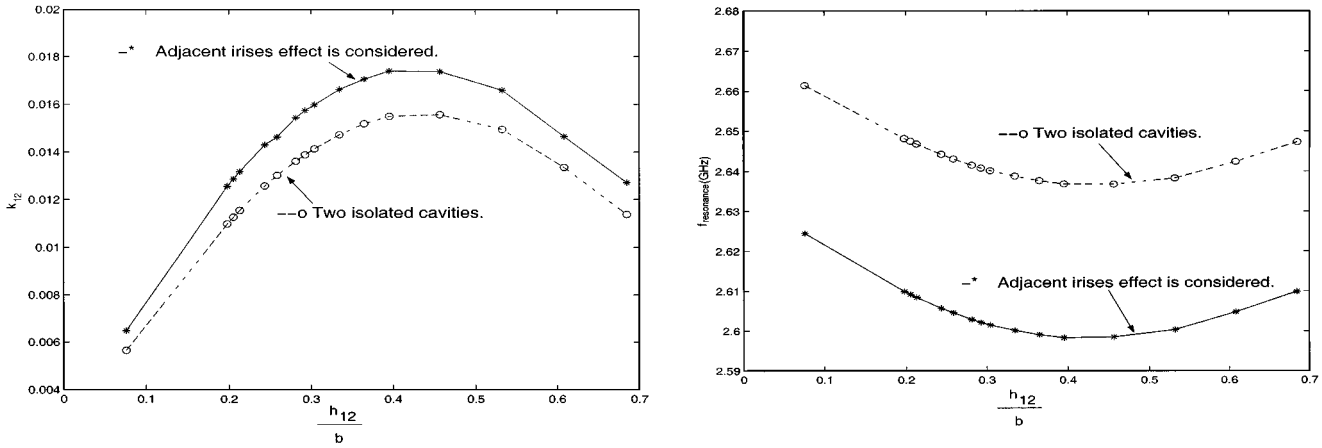

(a) (b)

Fig. 6. Effect of the iris height on the: (a) magnetic coupling and (b) resonant frequency. Dimensions as in Fig. 1: $b_{22} = 0.3439$ in, $W_{12} = 0.435$ in, $h_{12} = h_{12}$, $y_{o12} = b - h_{12}/2$, $W_{23} = 0.4$ in, $h_{23} = 0.271$ in, $y_{o23} = 1.1795$ in, $W_{14} = 0.75$ in, $h_{14} = 0.54$ in, $y_{o14} = 0.27$ in.

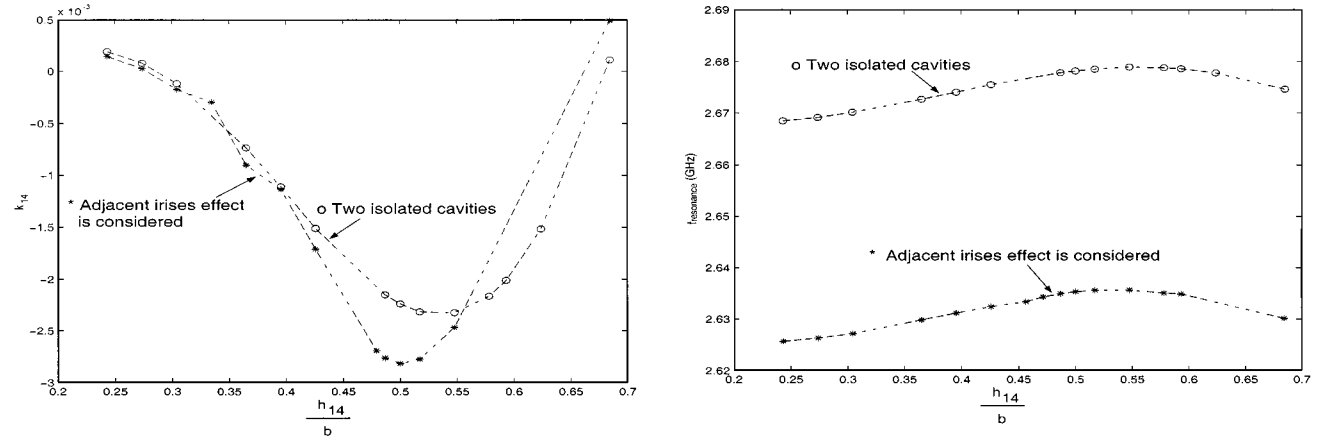

(a) (b)

Fig. 7. Effect of the iris height on the: (a) electric coupling and (b) resonant frequency. Dimensions as in Fig. 1: $b_{22} = 0.3439$ in, $W_{12} = 0.435$ in, $h_{12} = 0.385$ in, $y_{o12} = 1.1225$ in, $W_{23} = 0.4$ in, $h_{23} = 0.271$ in, $y_{o23} = 1.1795$ in, $W_{14} = 0.75$ in, $h_{14} = h_{14}$, $y_{o14} = h_{14}/2$.

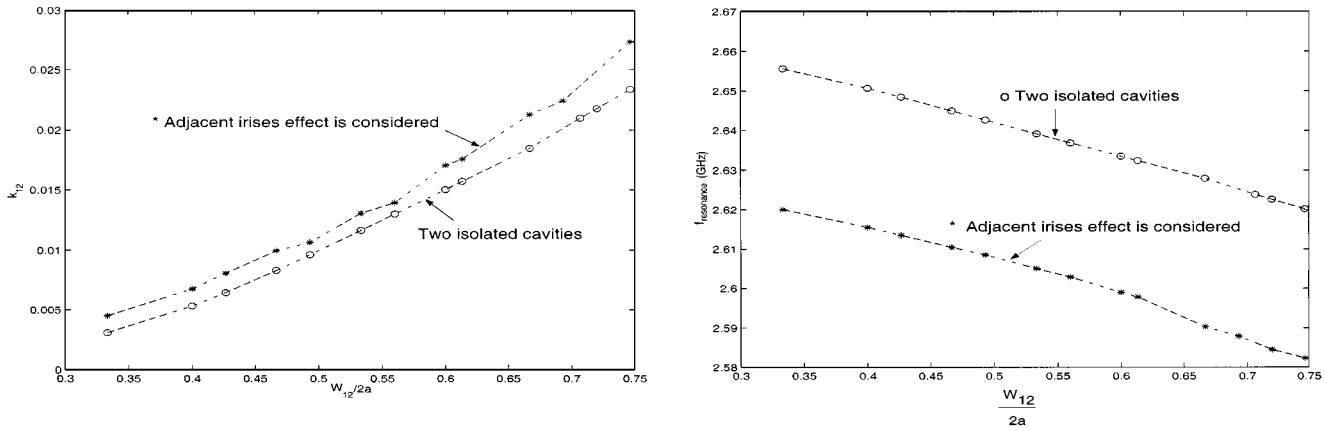

(a) (b)

Fig. 8. Effect of the iris width on the: (a) magnetic coupling and (b) resonant frequency. Dimensions as in Fig. 1: $b_{22} = 0.3439$ in, $W_{12} = W_{12}$, $h_{12} = 0.385$ in, $y_{o12} = 1.1225$ in, $W_{23} = 0.4$ in, $h_{23} = 0.271$ in, $y_{o23} = 1.1795$ in, $W_{14} = 0.75$ in, $h_{14} = 0.54$ in, $y_{o14} = 0.27$ in.

to the variation of the post length that controls the resonant frequency. Fig. 10(a) shows the effect of the post gap on the negative coupling where the coupling increases as the post gap increases up to a maximum value for $b_{21}/b = 0.25$, after which the coupling decreases as the post gap increases. The negative coupling, when the adjacent irises' effect is considered, is larger than the one obtained from two isolated cavities. Fig. 10(b) shows the variation of the resonant frequency for the case of negative coupling as a function of the post gap. The resonant frequency increases with the post gap. This curve indicate which

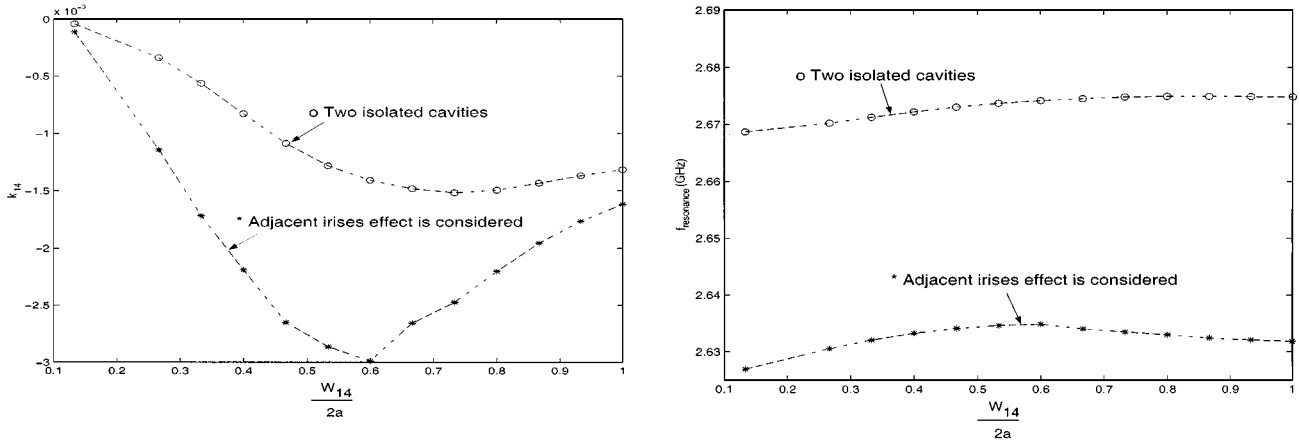

(a) (b)

Fig. 9. Effect of the iris width on the: (a) electric coupling and (b) resonant frequency. Dimensions as in Fig. 1: $b_{22} = 0.3439$ in, $W_{12} = 0.435$ in, $h_{12} = 0.385$ in, $y_{o12} = 1.1225$ in, $W_{23} = 0.4$ in, $h_{23} = 0.271$ in, $y_{o23} = 1.1795$ in, $W_{14} = W_{14}$, $h_{14} = 0.54$ in, $y_{o14} = 0.27$ in.

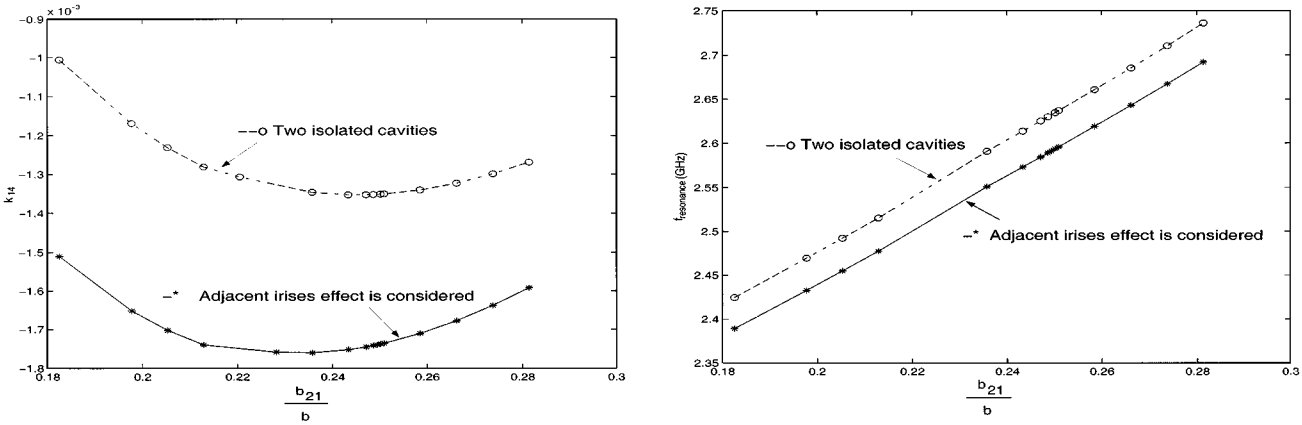

(a) (b)

Fig. 10. Effect of the post gap on the: (a) electric coupling and (b) resonant frequency. Dimensions as in Fig. 1: $W_{12} = 0.435$ in, $h_{12} = 0.385$ in, $y_{o12} = 1.1225$ in, $W_{23} = 0.4$ in, $h_{23} = 0.271$ in, $y_{o23} = 1.1795$ in, $W_{14} = 0.75$ in, $h_{14} = 0.54$ in, $y_{o14} = 0.27$ in.

post gap should be used to compensate for the resonant frequency reduction due to the loading effect. Fig. 11 shows the effect of varying the post length of the second and third cavities (the post length of the first and fourth cavities is held fixed) on the shift of each cavity resonant frequency from the desired center frequency of the filter. This curve shows that there is a unique post length giving a minimum equal shift (Δ) for all cavities, i.e., all the cavities are synchronously tuned. Practically, the coupling and resonant frequency can be adjusted by varying the post gap and by inserting a coupling screw in the iris between each two cavities, respectively. Fig. 12(a) shows the effect of the coupling screw length d_s on the coupling between two identical cavities. The coupling increases as the screw goes deeper into the iris. Fig. 12(b) shows the corresponding cavity resonant frequency variation. Fig. 13 shows the effect of the partial post height b_1 on the negative coupling. As b_1 increases, the coupling switches from negative to positive coupling.

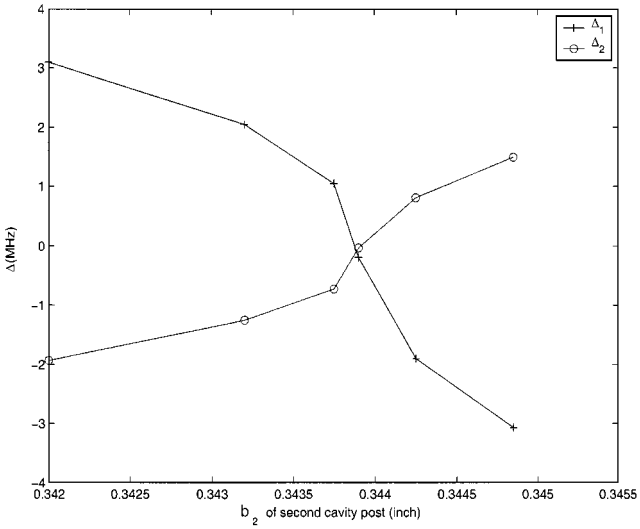

Fig. 11. Shift of each cavity resonant frequency from the filter center resonant frequency as a function of the gap of the second cavity post. Iris 1–2: 0.433 in $\times$ 0.385 in. Iris 2–3: 0.4 in $\times$ 0.271 in, Iris 1–4: 0.75 in $\times$ 0.54 in.

D. Nonadjacent Coupling

Fig. 14 shows the variation of the adjacent and nonadjacent coupling as a function of the iris width. The structure, shown in the figure inset, is symmetric around the symmetry plane A–A. The curves show that the couplings are increasing as the iris width increases. For this case, the nonadjacent coupling is very small compared to the adjacent coupling. Fig. 15 shows the effect of the

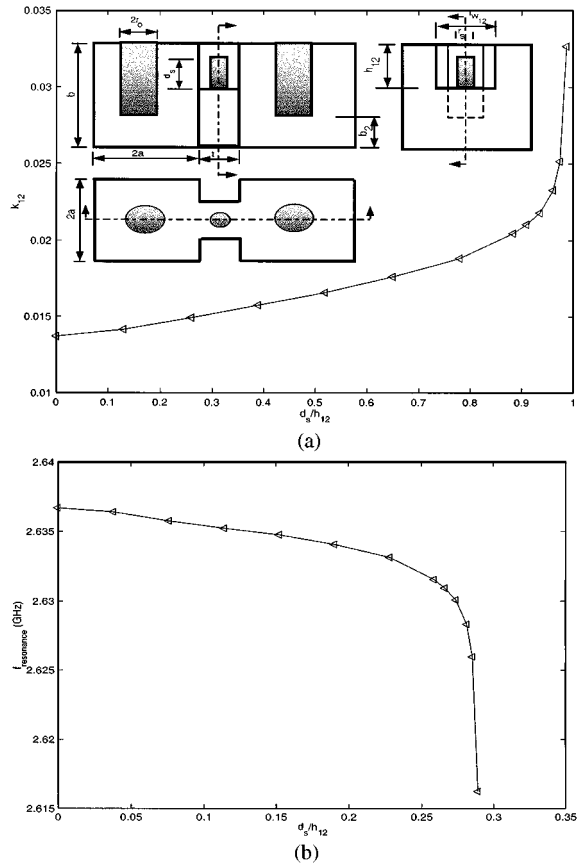

Fig. 12. (a) Variation of the coupling between two isolated cavities as a function of the coupling screw length. (b) Variation of the resonant frequency as a function of the coupling screw length. $W_{12} = 0.435$ in, $h_{12} = 0.385$ in, $2a = 0.75$ in, $b = 1.315$ in, $t = 0.1$ in, $b_2 = 0.3439$ in, $r_o = 0.115$ in, $r_s = 0.045$ in.

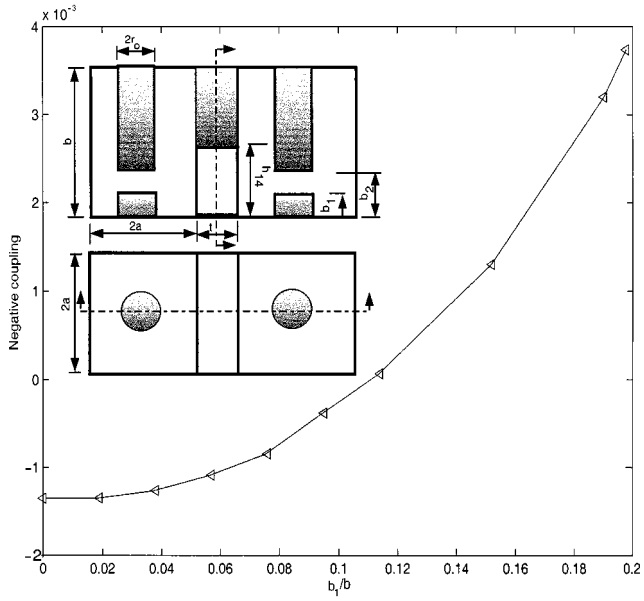

Fig. 13. Negative coupling between two isolated cavities as a function of the partial post height. $h_{14} = 0.54$ in, $2a = 0.75$ in, $b = 1.315$ in, $t = 0.1$ in, $b_2 = 0.3439$ in, $r_o = 0.115$ in.

iris width on the adjacent and nonadjacent couplings for the case of three coupled cavities forming a right-hand corner, as shown in the inset figure, as the iris width increases, the couplings are

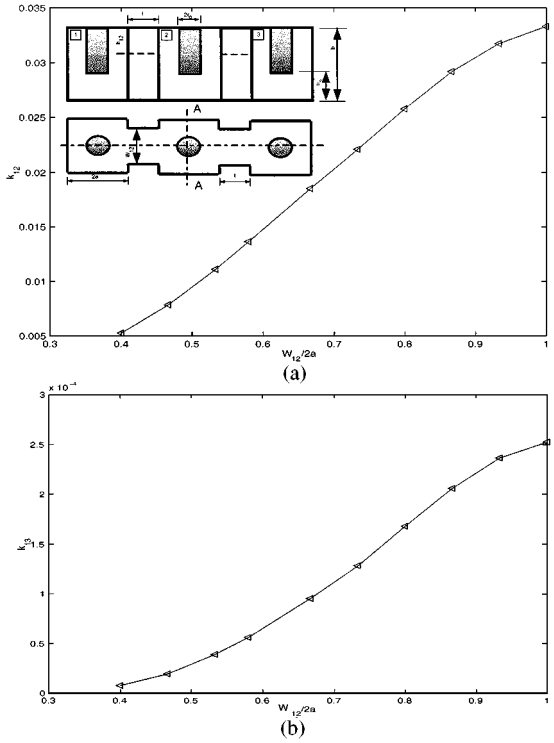

Fig. 14. Adjacent (k_{12}) and nonadjacent (k_{13}) couplings for the case of three combline cavities lined up and coupled through coupling irises. Dimensions as shown in the figure: $2a = 0.75$ in, $b = 1.315$ in, $2r_o = 0.23$ in, $t = 0.1$ in, $b_2 = 0.3439$ in, $h_{12} = 0.385$ in.

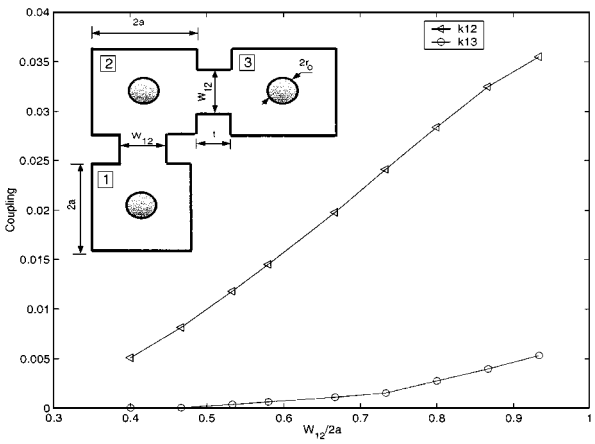

Fig. 15. Adjacent (k_{12}) and nonadjacent (k_{13}) couplings for the case of three combline cavities forming a right corner and coupled through coupling irises. Dimensions as shown in the figure: $2a = 0.75$ in, cavity height $= 1.315$ in, $2r_o = 0.23$ in, $t = 0.1$ in, post gap $= 0.3439$ in, iris height $= 0.385$ in.

increasing. The nonadjacent coupling for the case of three coupled cavities forming a right-hand corner is larger than the one where the three coupled cavities are lined up.

E. Design Example

As an application of the modeling, a four-pole slot-coupled combline filter centered at 2.595 GHz with 29-MHz bandwidth is designed. To realize the design by combline cavities, the schematic configuration shown in Fig. 1 is used. The top plane in the configuration is the ground plane. The input and output coupling of the filter are realized by a tapped-in 50-Ω coaxial line. The tap-in position that gives the required coupling is

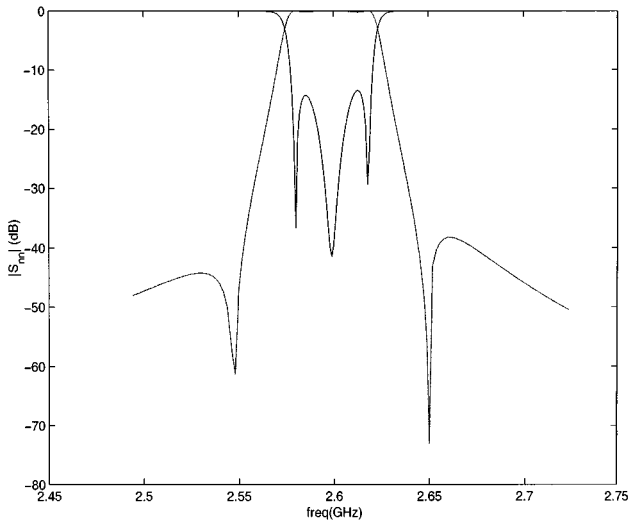

Fig. 16. Four-pole elliptic filter initial frequency response. Dimensions as in Fig. 1: $W_{12} = 0.433$ in, $h_{12} = 0.385$ in, $y_{o12} = 1.1225$ in, $W_{23} = 0.4$ in, $h_{23} = 0.271$ in, $y_{o23} = 1.1795$ in, $W_{14} = 0.75$ in, $h_{14} = 0.54$ in, $y_{o14} = 0.27$ in, $2a = 0.75$ in, $b = 1.315$ in, $t = 0.1$ in, $r_o = 0.115$ in, $b_{21} = 0.32$ in, $b_{22} = 0.3439$ in.

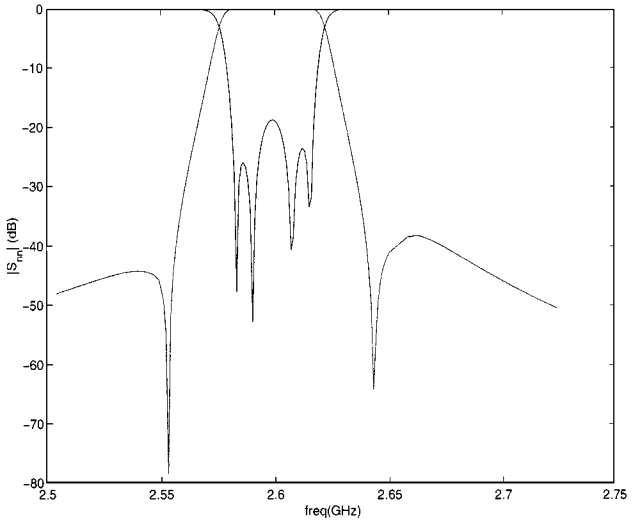

Fig. 17. Four-pole elliptic filter optimized frequency response. Dimensions as in Fig. 1: $W_{12} = 0.435$ in, $h_{12} = 0.385$ in, $y_{o12} = 1.1225$ in, $W_{23} = 0.4$ in, $h_{23} = 0.27$ in, $y_{o23} = 1.18$ in, $W_{14} = 0.75$ in, $h_{14} = 0.541$ in, $y_{o14} = 0.2705$ in, $2a = 0.75$ in, $b = 1.315$ in, $t = 0.1$ in, $r_o = 0.115$ in, $b_{21} = 0.32$ in, $b_{22} = 0.3439$ in.

found by using HFSS.[1] The initial slot dimensions are determined by the method described in the previous section to give the required coupling for each slot. The coupling matrix to be realized is given by

$$M = \begin{bmatrix} 0 & 0.9799 & 0 & -0.1095 \\ 0.9799 & 0 & 0.7875 & 0 \\ 0 & 0.7875 & 0 & 0.9799 \\ -0.1095 & 0 & 0.9799 & 0 \end{bmatrix}$$

$$R_1 = R_4 = 1.2535.$$

The initial filter response is shown in Fig. 16. Fig. 17 shows the optimized response of the four-pole elliptic function filter. After optimization, all the cavities are synchronously tuned with resonant frequency equal to 2.599 GHz.

[1]Agilent HFSS 5.5, Agilent EEsof EDA, Palo Alto, CA, 1999.

IV. Conclusion

A rigorous method for computing the generalized scattering matrix of conducting posts in rectangular waveguide junctions has been presented. By cascading the generalized scattering matrices of the different building blocks, accurate coupling between combline cavities in the presence of other couplings has been investigated. The effect of changing iris dimensions and position on the coupling and resonant frequency values has been obtained. A comparison has been done between values obtained for two isolated cavities and two cavities in the presence of other couplings. Numerical results has shown that the resonant frequency when the adjacent couplings effect is considered has a large variation from that of two isolated cavities. The adjacent and nonadjacent couplings have been rigorously investigated for different configurations of three coupled cavities.

References

[1] G. L. Matthaei, "Comb-line band-pass filters of narrow or moderate band-width," *Microwave J.*, vol. 6, pp. 82–91, Aug. 1963.
[2] H.-W. Yao, K. A. Zaki, A. E. Atia, and R. Hershtig, "Full-wave modeling of conducting posts in rectangular waveguides and its applications to slot coupled combline filters," *IEEE Trans. Microwave Theory Tech.*, vol. 43, pp. 2824–2830, Dec. 1995.
[3] ——, "Generalized slot coupled combline filters," in *IEEE MTT-S Int. Microwave Symp. Dig.*, vol. 2, 1995, pp. 395–398.
[4] H.-W. Yao, "EM simulation of resonant and transmission structures applications to filters and multiplexers," Ph.D dissertation, Elect. Comput. Eng. Dept., Univ. Maryland at College Park, College Park, MD, 1995.
[5] J. Pace and R. Mittra, "Generalized scattering matrix analysis of waveguide discontinuity problems," in *Quasi-Optics XIV*. Brooklyn, NY: Polytech. Inst. Brooklyn Press, 1964, pp. 172–194.
[6] G. R. Simpson, "A generalized n-port cascade connection," in *IEEE MTT-S Int. Microwave Symp. Dig.*, 1981, pp. 507–509.
[7] Y.-C. Shih, T. Itoh, and L. Q. Bui, "Computer-aided design of millimeter-wave E-plane filters," *IEEE Trans. Microwave Theory Tech.*, vol. MTT-31, pp. 1135–1142, Feb. 1983.
[8] A. S. Omar and K. Schünemann, "Transmission matrix representation of finline discontinuities," *IEEE Trans. Microwave Theory Tech.*, vol. MTT-33, pp. 765–770, Sept. 1985.
[9] Y. Kobayashi and M. Minegishi, "Precise design of a bandpass filter using high-Q dielectric ring resonators," *IEEE Trans. Microwave Theory Tech.*, vol. MTT-35, pp. 1156–1160, Dec. 1987.
[10] S.-W. Chen and K. A. Zaki, "Dielectric ring resonators loaded in waveguide and on substrate," *IEEE Trans. Microwave Theory Tech.*, vol. 39, pp. 2069–2076, Dec. 1991.
[11] M. El Sabbagh and K. Zaki, "Modeling of rectangular waveguide junctions containing cylindrical posts," *Progress Electromag. Res.*, vol. PIER 33, pp. 299–331, 2001.
[12] R. Mittra and S. W. Lee, *Analytic Techniques in the Theory of Guided Waves*. New York: Macmillan, 1971.
[13] R. R. Mansour and R. H. MacPhie, "An improved transmission matrix formulation of cascaded discontinuities and its application to E-plane circuits," *IEEE Trans. Microwave Theory Tech.*, vol. MTT-34, pp. 1490–1498, Dec. 1986.
[14] J. Schwinger and D. S. Saxon, *Discontinuities in Waveguides: Notes on Lectures by Julian Schwinger*. New York: Gordon and Breach, 1968.

Mahmoud El Sabbagh (S'93) received the B.S. and M.S. degrees in electrical engineering from Ain Shams University, Cairo, Egypt, in 1994 and 1997, respectively, and is currently working toward the Ph.D. degree at the University of Maryland at College Park.

From 1994, 1997, he was a Lecturer in the Department of Electrical Engineering, Ain Shams University, where his research dealt with applications of superconductors in microwave circuits. Since 1998, he has been with the Microwave Group, University of Maryland at College Park. His research interests include electromagnetics, microwave circuits, simulation, and computer-aided design of microwave devices.

Kawthar A. Zaki (SM'85–F'91) received the B.S. degree (with honors) from Ain Shams University, Cairo, Egypt, in 1962, and the M.S. and Ph.D. degrees from the University of California at Berkeley, in 1966 and 1969, respectively, all in electrical engineering.

From 1962 to 1964, she was a Lecturer in the Department of Electrical Engineering, Ain Shams University. From 1965 to 1969, she was a Research Assistant in the Electronics Research Laboratory, University of California at Berkeley. In 1970, she joined the Electrical Engineering Department, University of Maryland at College Park, where she is currently a Professor of electrical engineering. Her research interests are in the areas of electromagnetics, microwave circuits, simulation, optimization, and computer-aided design of advanced microwave and millimeter-wave systems and devices. She has authored or co–authored over 200 publications and holds five patents on filters and dielectric resonators.

Prof. Zaki was the recipient of several academic honors and awards for teaching, research, and inventions.

Hui-Wen Yao (S'92–M'95–SM'97) received the B.S. and M.S. degrees from the Beijing Institute of Technology, Beijing, China, in 1983 and 1986, respectively, and the Ph.D degree from the University of Maryland at College Park in 1995, all in electrical engineering.

From 1986 to 1991, he was a Lecturer in the Department of Electrical Engineering, Beijing Institute of Technology, where his research dealt mainly with electromagnetic (EM) radiation, scattering, and antenna design. From 1992 to 1995, he was a Research Assistant in the Department of Electrical Engineering, University of Maryland at College Park, where he was involved with the analysis, modeling, and design of microwave and millimeter-wave devices and circuits. In 1995, he joined CTA Inc. Since 1997, he has been with the Orbital Sciences Corporation, Germantown, MD, where he is responsible for satellite communications systems. He has authored or co-authored 50 technical papers.

Dr. Yao is on the Editorial Board of the IEEE TRANSACTIONS ON MICROWAVE THEORY AND TECHNIQUES. He was the recipient of the 1998 Outstanding Technical Achievement Award presented by the Orbital Science Corporation.

Ming Yu (S'90–M'93–SM'01) received the Ph.D degree in electrical engineering from the University of Victoria, Victoria, BC, Canada.

In 1993, he joined ComDev Inc., Cambridge, ON, Canada, as a Member of Technical Staff, where he was been involved in the design of passive microwave hardware from 500 MHz to 60 GHz, insuring compliance with specifications, costs, and schedules. He was also a Principal Developer of a variety of ComDev Inc. proprietary software for microwave filters and multiplexers. His experience also includes being the Manager of filter/multiplexer technology (Space Group), Manager of test engineering, and Staff Scientist of corporate research and development. He is currently the Director of the Research and Development Programs of the Corporate Research and Development Department. He is responsible for overseeing the development of RF microelectromechanical (MEMS) technology, computer-aided tuning and EM modeling of microwave filter/multiplexer for wireless applications. He has authored or co–authored 15 publications and has three patents pending.

Dr. Yu was the recipient of the 1995 ComDev Achievement Award for the development of a computer-aided tuning (CAT) technique for microwave filters and multiplexers.